MONOPOD HOPPING ON ROUGH PLANETARY ENVIRONMENTS

Vasileios Vasilopoulos, Iosif S. Paraskevas, Evangelos Papadopoulos

Control Systems Laboratory, Department of Mechanical Engineering, National Technical University of Athens,

9, Heroon Polytexneiou Str., 15780 Zografou, Athens, Greece

Email: vasilis.vasilop@gmail.com, isparas@mail.ntua.gr, egpapado@central.ntua.gr

ABSTRACT

Recent successes of missions such as the MSL and the Rosetta have increased the interest in the robotic exploration of other planets and asteroids. Although most of these missions envisage the use of rovers, legged robots have shown the potential to outperform wheeled vehicles on rough terrains in terms of speed and energy efficiency. In this paper, the x-MP controller presented in recent work, is used to evaluate the performance of a monopod robot under the effect of different gravitational fields and terrain types. The performance of the x-MP controller during regulating the robot motion on rough terrains and for the exploration of different types of planetary environments will be examined using simulations. Additionally using the Cost of Transport index, useful conclusions regarding the performance of legged robots for planetary exploration will be extracted.

1. INTRODUCTION

Legged robots offer a great potential for traversing rough and unstructured environments in terms of speed and energy efficiency. Planets and asteroids are of great scientific and exploration interest and are characterized by such environments; therefore they are candidates for legged robot deployment. However, control requirements for legged robots are very demanding, especially when the terrain profile is rough.

An interesting approach towards running on rough terrains was introduced with the RHex robot [1], which uses open-loop control, thus forward speed is not controlled tightly. In addition, the robot ASTRO, part of an emulation testbed for asteroid exploration, was introduced as a six-limbed ambulatory locomotion system that replicates walking gaits of the arachnid insects [2]. On the other hand, DFKI researchers presented the SpaceClimber, a biologically inspired six-legged robot for steep slopes, and focused on the foot-design to handle constraints from the environmental ground conditions [3].

A common control strategy used by quadrupeds for traversing rough terrains involves footstep planning.

LittleDog has shown impressive results on significantly uneven terrain [4]. However, it is capable of static walking only. StarlETH also uses a similar approach [5]; a foot placement algorithm along with distribution of virtual forces among the stance legs is used to overcome unexpected obstacles and reject perturbations.

Interestingly, despite the increasing complexity in the development of control algorithms for legged robots, many studies disregard the effect of terrain compliance and permanent deformation. For example, for the monopod hopping robot in [6], the ground was considered completely stiff. For the MIT Cheetah 2, the authors determine a target ground force profile according to the desired duty cycle and stride duration, [7]. Again, the terrain is considered stiff and completely flat. On the other hand, the case of rough terrain is considered and a control algorithm is proposed for a monopod robot on rough terrain that could handle inclinations up to 20 deg in [8]. The robot was considered to possess two actuators, at its prismatic and rotational joint. Our recent work involved the development of a novel energy-based controller for a monopod hopping robot running over compliant terrains, [9]. This controller is capable of achieving and retaining a desired forward speed and main body apex height, using a *single* actuator located at the robot hip.

To this end, modelling of the foot-terrain interaction is an important aspect for control design, especially when designing robots and algorithms for autonomous exploration. In many works, a stiff revolute joint is used to represent the stance phase, disregarding ground interactions. Different approaches are necessary to assess its effects. This can be seen in works like [10], where a viscoelastic model is used, and like [11], where a terradynamics approach is employed. Similar approaches can be found in [12]. A viscoplastic model has been proposed, which enables the assessment of the effects of terrain permanent deformations on fast dynamic walking, [9].

In this paper, the description of the viscoplastic approach is briefly introduced and the x-MP controller is presented and used to evaluate the performance of the

monopod robot under the effect of *different gravitational fields* and *terrain types*. Using simulation results, the performance of the x-MP controller for regulating the robot motion on rough terrains and for the exploration of different types of planetary environments will be tested. The case of crater-like and unstructured terrain will be considered, without affecting the generality of the conclusions. In addition, using the Cost of Transport (CoT) index, the correlation between the energetic efficiency of the controller and the acceleration of gravity will be presented and useful conclusions regarding the choice of legged robots used for planetary exploration will be extracted.

2. CONTACT MODEL DESCRIPTION

2.1. Viscoplastic Contact Model

Any foot-terrain interaction model must represent realistically the robot behaviour, while running on deformable terrains. Main parameters affecting the motion of the robot include the compliance of the ground, the depth of the permanent deformation that may occur, and the change of characteristics due to repetitive loading on a particular point (i.e. ground compaction or similar phenomena). In the terramechanics approach, it is assumed that a wheel or a foot are in contact with the ground for considerable amount of time or permanently. For example, such approach is widely used in space technology for modeling the contact of rover wheels with the ground. This approach, however, cannot be applied to the case of fast dynamic running, as in this case.

Therefore, to represent the interaction of a monopod with the ground during running on compliant terrains accurately, a viscoplastic contact model was proposed, [9]. This model is considered to be an extension of non-linear viscoelastic contact models, and is based on the Hunt-Crossley (HC) model [12]. According to the proposed model, the interaction force F_g between the foot and the ground at stance instance i

$$F_g^i\left(y_g, \dot{y}_g\right) = \begin{cases} F_c^i = \left(\lambda_c^i k_g + b_g \dot{y}_g\right)\left(y_g - y_e^{i-1}\right)^n, \ \dot{y}_g \geq 0 \\ F_r^i = \left(\lambda_r^i k_g + b_g \dot{y}_g\right)\left(y_g - y_e^i\right)^n, \ \dot{y}_g < 0 \end{cases} \quad (1)$$

where the subscript c stands for compression and r for restitution, y_e is the depth reached at the end of impact, k_g and b_g are the stiffness and damping coefficients respectively, n in the case of Hertzian non-adhesive contact is equal to 1.5, and y_g is the depth of penetration. Note that k_g represents the equivalent stiffness between the materials in contact (i.e. in this case between the foot and the terrain), [13]. Damping is affected by the stiffness, as [14],

$$b_g = 1.5 \cdot c_a \cdot k_g \quad (2)$$

where c_a is usually between 0.01-0.5 depending on the materials and impact velocity. Throughout this work the value of c_a is considered to be equal to 0.2, without affecting the generality of conclusions.

To account for successive impacts at the same horizontal point, the index i is used to identify an impact instance, as the terrain inherits the characteristics from the previous impact instant due to permanent deformations. The effect of these is described with the *Coefficient of Permanent Terrain Deformation*, λ, which is defined in recursive form as:

$$\lambda_c^i = \begin{cases} 1, \quad i = 1 \\ \lambda_r^{i-1}, \quad i > 1, \quad i \in \mathbb{N} \end{cases} \quad (3)$$

$$\lambda_r^i = \lambda_r^i\left(materials, velocity, i\right), \quad i \in \mathbb{N}$$

where $\lambda_c^i \geq \lambda_r^i \geq 1$. Note that as the same terrain point is compressed, it becomes stiffer, [9]. To model this phenomenon, the following model is proposed for λ,

$$\lambda_r^i = 1 + a(i) \cdot \left(1 - e^{-i \cdot \beta(i)}\right), \quad i \in \mathbb{N} \quad (4)$$

where $a(i)$, $\beta(i)$ are functions of the impact instance i, of the materials and of the velocity. Parameter a sets the maximum value of λ_r^i, whereas an increase in β increases the speed of reaching this value.

The final depth y_e^i at the ith impact can be calculated by observing that at the maximum compression, $y_{c,max}^i$, the following applies,

$$y_{c,max}^i \Leftrightarrow F_c^i = F_r^i \quad \text{and} \quad \dot{y}_g = 0 \quad (5)$$

Using (1), one can deduce that

$$y_e^i = y_{c,max}^i \cdot \left(1 - \sqrt[n]{\lambda_c^i / \lambda_r^i}\right) + y_e^{i-1} \cdot \left(\sqrt[n]{\lambda_c^i / \lambda_r^i}\right) \quad (6)$$

where $y_e^0 = 0$ for consistency.

2.2. Friction

When the foot touches the ground, it may slip, depending on the touchdown angle and velocity and the materials in contact [15]. In order to evaluate the foot behavior during stance, a friction description is required. Here, the classical Static-plus-Coulomb model is implemented, which produces satisfactory results with reasonable computations, [16]. According to this model the friction force F_t is

$$F_t = \begin{cases} -\mu_c \cdot F_g \cdot \text{sgn} \dot{x}_g, \quad \dot{x}_g \neq 0 \\ -\left|F_\parallel\right| \text{sgn} F_\parallel, \quad \left|F_\parallel\right| < \mu_s \left|F_g\right|, \quad \dot{x}_g = 0, \quad \ddot{x}_g \neq 0 \end{cases} \quad (7)$$

where $\dot{x}_g$, $\ddot{x}_g$ are the velocity and acceleration

components of the foot which are parallel to the tangential plane between the foot and the ground, F_g is the interaction force from which is normal to the same tangential plane, $F_\parallel$ is the vectorial sum of all other forces applied, parallel to this tangential plane, and μ_c and μ_s are the Coulomb and static friction coefficients.

3. MONOPOD ROBOT DYNAMICS MODEL

The model of a monopod robot with a single actuator, which included the description of the foot-terrain interaction, was presented in [9]. Here, the system model is extended by means of taking friction into consideration and describing the motion of the robot over rough terrain including small inclinations. In this work, the following assumptions are used: (i) a point contact occurs each time the foot touches the ground as the foot is considered to be a point mass, (ii) bulldozing effects are neglected, (iii) the actuator is torque constrained, and (iv) the pitching motion of the body is bounded, in accordance to the experimental setup presented in [6].

The monopod robot model is shown in Fig. 1. It consists of a mass M corresponding to the robot body and a mass m corresponding to the equivalent mass of the robot leg and foot. The leg is springy with free length L and length at any time l, while the stiffness of the linear spring is k. The energy losses due to viscous friction in the leg prismatic degree of freedom (dof) are modelled with a damping coefficient b, while the leg angle with respect to the vertical is γ and the torque applied by the actuator at the body hip is τ. Table 1 summarizes robot and motion parameters.
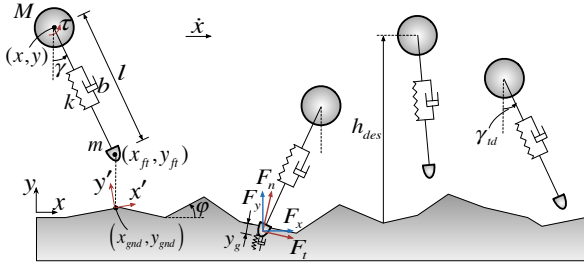

Figure 1. Model of the robot on rough surface.

The system variables for both the *flight phase*, where the foot does not touch the ground, and the *stance phase*, where the foot touches the ground, are the coordinates of the main body x, y, and the coordinates of the foot x_{ft}, y_{ft}. The equations of motion become (with $c\gamma = \cos\gamma$ and $s\gamma = \sin\gamma$)

$$M \cdot \ddot{x} + k \cdot (L - l) \cdot s\gamma - b \cdot \dot{l} \cdot s\gamma = -\tau \cdot l^{-1} \cdot c\gamma \qquad (8)$$

$$M \cdot \ddot{y} + M \cdot g - k \cdot (L - l) \cdot c\gamma + b \cdot \dot{l} \cdot c\gamma = -\tau \cdot l^{-1} \cdot s\gamma \qquad (9)$$

$$m \cdot \ddot{x}_{ft} - k \cdot (L - l) \cdot s\gamma + b \cdot \dot{l} \cdot s\gamma = \tau \cdot l^{-1} \cdot c\gamma + F_x \qquad (10)$$

$$m \ddot{y}_{ft} + mg + k (L - l) c\gamma - b \cdot \dot{l} \cdot c\gamma = \tau \cdot l^{-1} \cdot s\gamma + F_y \qquad (11)$$

where F_x, F_y are the ground contact forces in the horizontal and vertical direction respectively, defined in the inertial frame.

Table 1. Nomenclature.

Symbol	Quantity
x	Body CM x-axis coordinate
y	Body CM y-axis coordinate
l	Leg length
γ	Leg absolute angle
x_{ft}	Foot x-axis coordinate
y_{ft}	Foot y-axis coordinate
L	Leg free length
φ	Ground inclination
M	Body mass
k	Leg spring stiffness
b	Leg damping coefficient
m	Effective mass of leg and foot
τ	Hip torque
F_x	Ground force in horizontal direction
F_y	Ground force in vertical direction
F_t	Ground force in tangential direction
F_n	Ground force in normal direction

These forces are determined from the normal and tangential components of the contact force with respect to the common tangential plane between the foot and the ground, F_n and F_t, using the inclination φ as

$$F_x = -F_n \cdot \sin\varphi + F_t \cdot \cos\varphi \qquad (12)$$

$$F_y = F_n \cdot \cos\varphi + F_t \cdot \sin\varphi \qquad (13)$$

To implement the viscoplastic contact model and calculate the friction force, the foot position and velocity in the normal and the tangential directions must be calculated. For this reason, a local coordinate system (x', y') is defined with axes tangential and normal to the ground surface correspondingly. The origin of this system during the flight phase is always located at the point (x_{gnd}, y_{gnd}) of the terrain profile that is just below the horizontal foot position, as shown in Fig 1. During the stance phase, the origin of the system coincides with the point where the collision with the ground occurred. In this way, the foot position is being calculated in the

local coordinate system using the following transformation from the inertial coordinate system

$$\mathbf{r}' = \mathbf{T} \cdot \mathbf{r} \tag{14}$$

where $\mathbf{r}' = [\ x'_{ft}\ \ y'_{ft}\ \ 1\ ]^T$ contains the foot position in the local coordinate system, $\mathbf{r} = [\ x_{ft}\ \ y_{ft}\ \ 1\ ]^T$ contains the foot position in the inertial coordinate system and $\mathbf{T}$ is the transformation matrix from the inertial to the local coordinate system, given as (with $c\gamma = \cos\gamma$ and $s\gamma = \sin\gamma$)

$$\mathbf{T} = \begin{bmatrix} c\varphi & s\varphi & -x_{gnd} \cdot c\varphi - y_{gnd} \cdot s\varphi \\ -s\varphi & c\varphi & x_{gnd} \cdot s\varphi - y_{gnd} \cdot c\varphi \\ 0 & 0 & 1 \end{bmatrix} \tag{15}$$

Using (14), the foot velocity components in the normal and tangential directions $\dot{x}'_{ft}$, $\dot{y}'_{ft}$ are also determined as follows

$$\dot{x}'_{ft} = \dot{x}_{ft} \cdot \cos\varphi + \dot{y}_{ft} \cdot \sin\varphi \tag{16}$$

$$\dot{y}'_{ft} = -\dot{x}_{ft} \cdot \sin\varphi + \dot{y}_{ft} \cdot \cos\varphi \tag{17}$$

Based on assumption (i) and on the former analysis, the penetration depth y_g equals to the foot position y'_{ft} in the local system during stance, as shown in Fig. 1. Therefore, y'_{ft}, $\dot{y}'_{ft}$ substitute y_g, $\dot{y}_g$ in (1), while $\dot{x}'_{ft}$ substitutes $\dot{x}_g$ in (7). The stance phase begins with the foot initially touching the ground following a flight phase $(y'_{ft} = 0)$ and terminates when the ground force is zeroed $(F_n = 0)$. During the flight phase, the forces from the ground are zero $(F_n, F_t = 0)$.

4. CONTROL METHODOLOGY

A novel controller called *Extended Multipart (x-MP)* was presented in [9], that is capable of achieving and retaining a desired forward speed and main body apex height on any terrain, using only a single actuator at the robot hip. It uses energy principles and does not require an estimate of the terrain properties. However, its implementation is limited to completely flat terrains with no inclination. In this paper the x-MP is extended by means of achieving hopping on rough terrains with small inclinations of $\pm 5\deg$. Larger inclinations are possible, but require larger motor torques.

The controller in this work is applied just after each liftoff of the leg, when the stance phase of stride $j-1$ terminates and the flight phase of stride j begins. At that moment, it calculates a desired touchdown angle γ_{td}^j for stride j and a constant torque τ_s^j to be applied during the stance phase of stride j. The controller performs its calculations in three steps, as described in the following sections.

4.1. Prediction of next touchdown ground point

The first action of the controller is to predict the point of the ground surface on which the leg touchdown of stride j will occur. In general the terrain profile is described by a function $y_{gnd} = f(x_{gnd})$, which is unknown to the robot. By estimating the next touchdown point, the control algorithms developed for flat terrain can then be applied. The basic idea for this estimation is depicted in Fig. 2, where the touchdown instants of strides $j-2$ and $j-1$, as well as the estimated touchdown instant of stride j are shown.
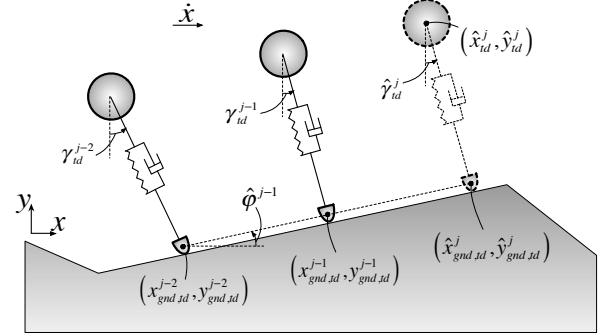

Figure 2. Touchdown ground point estimation concept.

To be more specific, after each touchdown of the robot leg, the terrain profile coordinates $x_{gnd,td}$ and $y_{gnd,td}$ at that point are calculated using the kinematic equations

$$x_{gnd,td} = x_{ft,td} = x_{td} + l_{td} \cdot \sin\gamma_{td} \tag{18}$$

$$y_{gnd,td} = y_{ft,td} = y_{td} - l_{td} \cdot \cos\gamma_{td} \tag{19}$$

where the subscript 'td' denotes the value of each magnitude at touchdown. Relying on the response of the previous two strides and using (18) and (19), the controller estimates the terrain inclination of the stride $j-1$ as follows

$$\hat{\varphi}^{j-1} = \tan^{-1}\left(\frac{y_{gnd,td}^{j-1} - y_{gnd,td}^{j-2}}{x_{gnd,td}^{j-1} - x_{gnd,td}^{j-2}} \right) \tag{20}$$

with $(\hat{\#})$ denoting an estimated magnitude of $(\#)$. For the first and the second stride where no previous data exists, $\hat{\varphi}^0 = \hat{\varphi}^1 = 0$.

Next, the following assumptions are made for stride j: (i) due to small length strides the terrain inclination will remain the same, (ii) the touchdown angle will be approximated as being equal to the touchdown angle during stride $j-1$ so that $\hat{\gamma}_{td}^j \approx \gamma_{td}^{j-1}$ and (iii) the robot body performs a ballistic trajectory during flight. The goal is to estimate the touchdown point $(\hat{x}_{gnd,td}^j, \hat{y}_{gnd,td}^j)$ of the terrain profile. Using assumptions (ii) and (iii), the following set of equations can be formed regarding the ballistic trajectory of the main body (with $c\gamma = \cos\gamma$)

$$\hat{y}_{td}^{j} = \hat{y}_{gnd,td}^{j} + L\,\mathrm{c}\,\hat{\gamma}_{td}^{j} = y_{lo}^{j-1} + \dot{y}_{lo}^{j-1}\Delta\hat{t}_{f}^{j} - 0.5g\left(\Delta\hat{t}_{f}^{j}\right)^{2} \quad (21)$$

$$\hat{x}_{td}^{j} = \hat{x}_{gnd,td}^{j} - L\cdot\sin\hat{\gamma}_{td}^{j} = x_{lo}^{j-1} + \dot{x}_{lo}^{j-1}\cdot\Delta\hat{t}_{f}^{j} \quad (22)$$

with the subscript 'lo' denoting the value of each magnitude at liftoff and $\Delta\hat{t}_{f}^{j}$ the estimated duration of flight for the stride j. Using assumption (i), $\hat{x}_{gnd,td}^{j}$ and $\hat{y}_{gnd,td}^{j}$ are related according to the following equation

$$\hat{y}_{gnd,td}^{j} = y_{gnd,td}^{j-1} + \left(\hat{x}_{gnd,td}^{j} - x_{gnd,td}^{j-1}\right)\cdot\tan\hat{\varphi}^{j-1} \quad (23)$$

Equations (21), (22) and (23) formulate a 3x3 system, with $(\hat{x}_{gnd,td}^{j}, \hat{y}_{gnd,td}^{j}, \Delta\hat{t}_{f}^{j})$ being the unknown variables. This system can be analytically solved and yield the estimated point ($\hat{x}_{gnd,td}^{j}, \hat{y}_{gnd,td}^{j}$).

4.2. Calculation of desired touchdown angle

Following the calculation of $\left(\hat{x}_{gnd,td}^{j}, \hat{y}_{gnd,td}^{j}\right)$, the controller calculates the desired touchdown angle γ_{td}^{j}. In [9], a method was proposed where the extended robot model incorporating the foot-terrain description could be mapped to a simple model for stiff terrains by calculating an equivalent stiffness and damping k' and b' respectively, as shown in Fig. 3. The calculation of k', b' was performed using previous stride response and calculating the energy losses due to damping and ground dissipation. The desired touchdown angle γ_{td}^{j} was determined by integrating the flight and stance dynamics of the equivalent simple model, according to the desired main body apex height h_{des}.
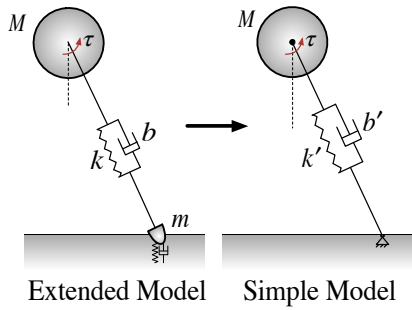
Figure 3. Idea of the x-MP controller.

The same control approach is used here, with the main difference that the ground level is now considered to be at $\hat{y}_{gnd,td}^{j}$ rather than at zero, and the desired main body apex height is determined so that a specific clearance from the ground $\Delta h_{cl,des}$ is reached, as follows

$$h_{des} = \Delta h_{cl,des} + \hat{y}_{gnd,td}^{j} \quad (24)$$

4.3. Calculation of constant stance torque

After the calculation of the desired touchdown angle, the x-MP determines a constant torque τ_{s}^{j} to be applied during the next stance phase. This torque is calculated so that a desired energy level is reached [9]. The controller compensates for leg damping energy losses and energy losses due to ground dissipation, and accelerates or decelerates the system according to the desired forward velocity $\dot{x}_{des}$ and apex height h_{des}. The same algorithm is used here.

Following these calculations, the leg is servoed to the desired touchdown angle γ_{td}^{j} during the flight phase using a PD controller as described in [9]. After the leg touchdown, which is determined using a force sensor at the robot foot, the constant torque τ_{s}^{j} is applied.

4.4. Discussion

The controller uses information from a force sensor yielding the ground reaction forces $\left(F_{n}, F_{t}\right)$ and from two encoders that measure the leg angle γ and the leg length l, and estimates the body position (x, y) using the robot dynamic model fused with data from an inertial sensor, [9]. No extra sensor for determining the terrain properties or inclination is required. Finally, the controller does not need tuning but only an estimate of the robot parameters.

5. SIMULATION RESULTS

To evaluate controller performance, various simulation scenarios were run, each for a different gravitational acceleration. The equivalent stiffness k_{g} between the materials in contact (i.e. foot and ground) was used [13], where the properties of various Earth terrains in [17] were used for the Moon and Mars also, without loss of generality of the conclusions.

The foot material was selected to be ether polyurethane with Young's modulus $E = 100\,\mathrm{MPa}$. Thus, as an example, the equivalent stiffness between this material and granite with Young's modulus $E = 50\,\mathrm{GPa}$ is $k_{g} \approx 450,000\,\mathrm{N/m}$. In this way, three main categories of terrains were examined: *soft* ground with $k_{g} = 8\cdot10^{4}\,\mathrm{N/m}$, $\mu_{s} = 0.5$ and $\mu_{c} = 0.4$, *moderate* ground with $k_{g} = 2\cdot10^{5}\,\mathrm{N/m}$, $\mu_{s} = 0.6$ and $\mu_{c} = 0.5$, and *stiff* ground with $k_{g} = 4\cdot10^{5}\,\mathrm{N/m}$, $\mu_{s} = 0.7$ and $\mu_{c} = 0.6$.

In all cases, the monopod hopping robot described in Section 3 was used. Its parameters are shown in Table 2. The acceleration of gravity g varied according to each motion scenario. The simulations were performed in Matlab using ode23s with absolute and relative tolerance 10^{-2} and maximum step 10^{-5}. To minimize the zero-crossing arithmetic problems created by the numerical stiffness, the impact was considered over when the interaction force between the foot and the terrain was below 5N, while the foot transition from slip to stick was considered to occur when the foot horizontal velocity was below $10^{-4}\,\mathrm{m/s}$.

Table 2. Robot parameters during simulation.

Parameter	Value
Main body mass M	4 kg
Equivalent foot mass m	0.5 kg
Leg length L	0.3 m
Leg spring stiffness k	12,000 N/m
Leg damping coefficient b	3 Ns/m

5.1. Controller performance

In Fig. 4 the response of the controller on a rough terrain profile on Mars ($g = 3.71$ m/s^2) with maximum inclination of ± 2 deg is shown. The initial conditions were: height $h_0 = 0.32$ m and forward velocity $\dot{x}_0 = 0.6$ m/s . The desired commands were clearance from the ground $\Delta h_{cl,des} = 0.32$ m and forward velocity $\dot{x}_{des} = 0.6$ m/s , while the ground was considered stiff. The simulations show that the controller, using the touchdown ground point estimation algorithm, retains the desired forward velocity and follows the desired apex height profile smoothly.
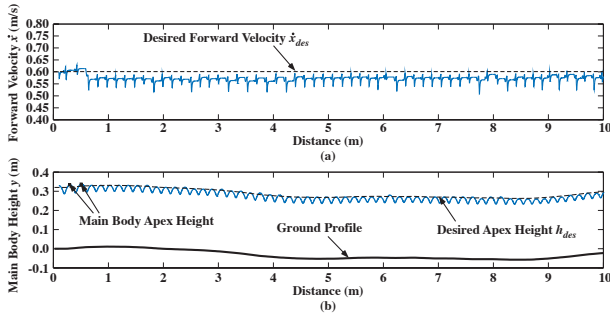
Figure 4. Controller performance on rough, random-generated terrain profile on Mars: (a) Forward Velocity, (b) Main Body Height.

The above simulation showed that the x-MP controller can be used for the successful motion of the monopod robot on the unstructured environment of another planet. However, in this motion scenario, the ground was considered completely stiff and with no permanent deformations. To extract further conclusions about the controller applicability on every type of terrain, a different set of simulations were performed on the shallow crater depicted in Fig. 5, where the terrain type gradually changed from stiff and non-deformable at the external sides of the crater, to soft and very deformable at the center of the crater.

The robot behavior was simulated for the Earth ($g = 9.81$ m/s^2), the Mars ($g = 3.711$ m/s^2) and the Moon ($g = 1.622$ m/s^2). The initial conditions and desired magnitudes remained the same as the previous scenario. The controller adapted quickly to each terrain

and followed the desired objectives of forward velocity and main body height in each case, as it is shown in Fig. 6. It can be observed that the response converged more slowly to the desired commands as the acceleration of gravity decreased. This is due to the fact that the flight phase duration was larger; in this way, there were fewer touchdowns for the same horizontal distance and the constant stance torque and touchdown angle, which are the inputs that regulate the system energy level, were applied less frequently.
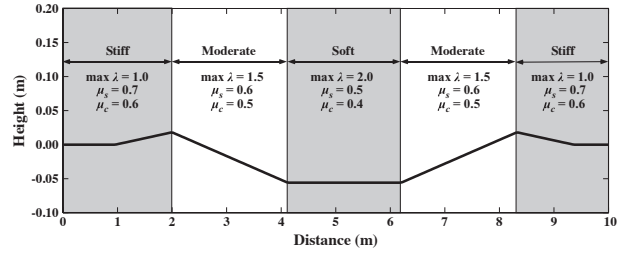

Figure 5. Terrain profile used for simulations.

5.2. Energy requirements and Cost of Transport

It is interesting to examine the controller behavior as the acceleration of gravity, the terrain type or the terrain inclination changes. For this reason, Fig. 7, containing information about the leg angle response and the commanded torques by the controller during the stance phase, is employed. Note that negative torque corresponds to positive work, since the leg moves in the negative direction during stance, which is desired. As can be seen, for all gravity accelerations, on the uphills, the controller sets larger touchdown angles and constant torques in order to retain the desired forward velocity.

On the contrary, when the robot ran downhill, the controller tried to decelerate the body and cancel the gravity effect; for this reason the touchdown angles and the constant torques were smaller in comparison to the uphill or flat motion. The controller outputs also depended on terrain properties. The more compliant and the more deformable was the ground, the larger the touchdown angles and stance torques were. As far as gravity is concerned, it can be seen that it did not generally affect the commanded touchdown angles. This was expected considering that the desired touchdown angle depends solely on the desired forward velocity and main body apex height and the initial conditions of the flight phase, which remained approximately the same. On the contrary, it can be noticed that greater acceleration of gravity resulted in greater stance torques, as the controller had to compensate for larger impact losses during stance.

To further evaluate the effect of gravity on the robot energy consumption, an additional number of simulations were performed on the same shallow crater shown in Fig. 5, for different values of the acceleration

of gravity g. In this work, the Cost of Transport (CoT) index was used, which is defined as follows

$$CoT = W \big/ \big[(M+m) \cdot g \cdot d \big] \qquad (25)$$

where W is the total work required over a distance d. Fig. 8 shows the total energy consumption by the robot's single actuator as a function of gravity. As can be seen, the total work W increased linearly with the acceleration of gravity. This was expected considering that greater acceleration of gravity resulted in larger energy losses during the impact with the ground, which the controller had to compensate for.
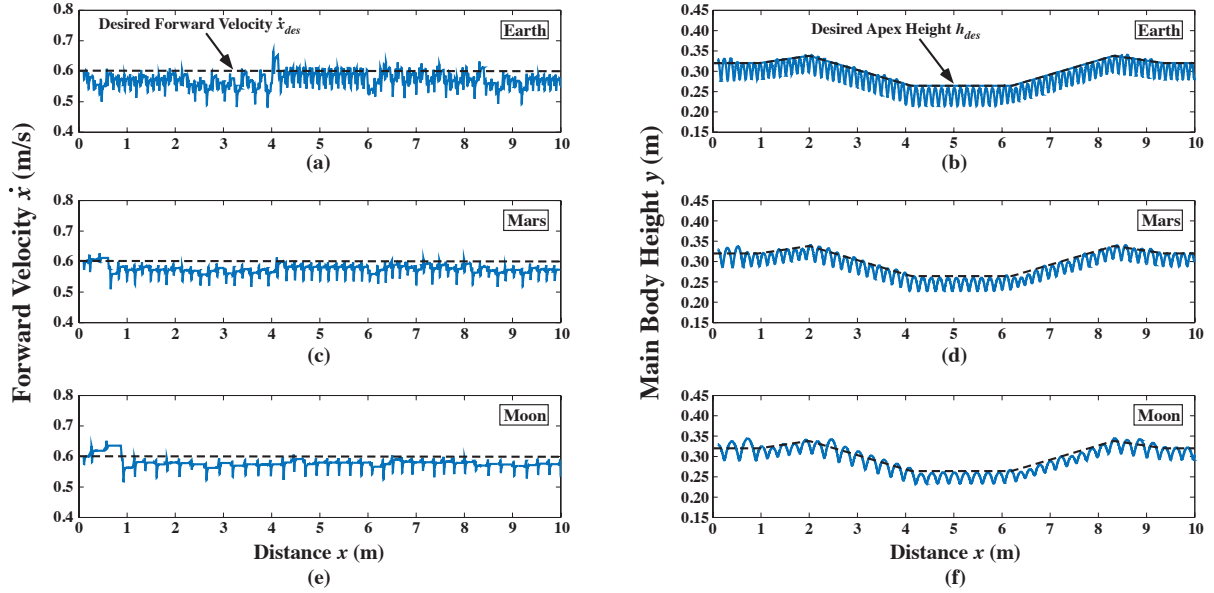
Figure 6. Controller performance on shallow crater: (a), (c), (e) Forward Velocity on Earth, Mars and Moon respectively, (b), (d), (f) Main Body Height on Earth, Mars and Moon respectively.
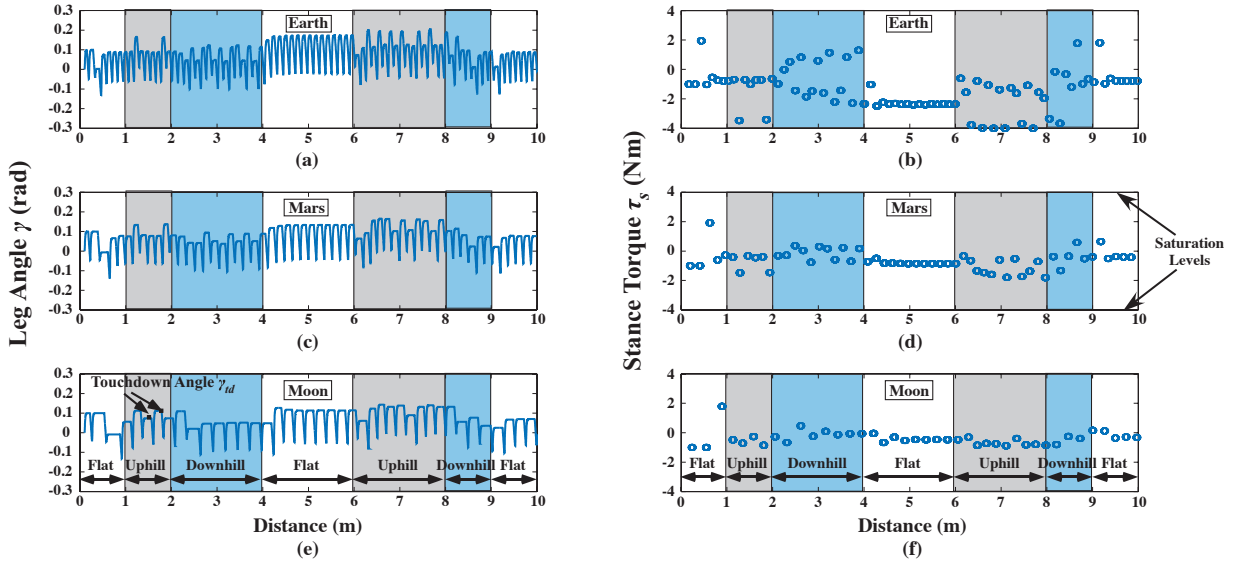

Figure 7. Controller behavior on shallow crater: (a), (c), (e) Leg Angle response on Earth, Mars and Moon respectively, (b), (d), (f) Commanded Stance Torques on Earth, Mars and Moon respectively.

On the other hand, Fig. 9 shows the effect of the acceleration of gravity on the Cost of Transport. As can be seen, the CoT index decreases when the acceleration of gravity increases. It can be also presumed that CoT remains almost constant beyond a specific threshold value for the acceleration of gravity. However, the total efficiency of the motion falls exponentially as the acceleration of gravity decreases. This must be taken

into consideration when planning exploration missions with legged robots on planets or other celestial bodies.
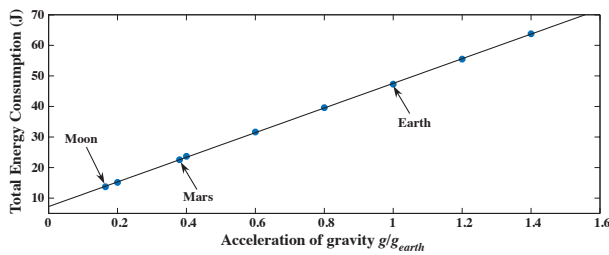

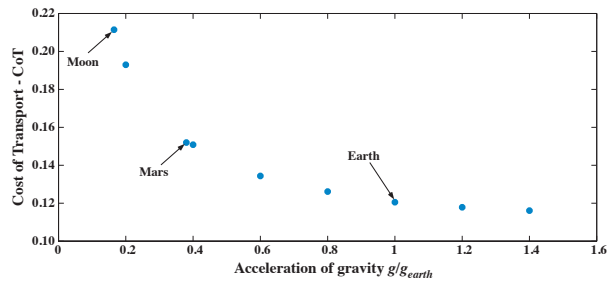**Figure 8**. The effect of gravity on energy consumption.

Figure 9. The effect of gravity on the Cost of Transport.

6. CONCLUSIONS

The performance of a monopod robot under the effect of different gravitational fields and terrain types was examined. First, a description of the viscoplastic approach was introduced and the x-MP controller was presented and used to evaluate the performance of the monopod robot. Using simulation results, the performance of the x-MP controller for regulating the robot motion on rough terrains and for the exploration of different types of planetary environments has been tested. The use of the Cost of Transport (CoT) index to correlate the energetic efficiency of the controller and the acceleration of gravity was presented and useful conclusions were extracted. The results of this paper give insights that should be taken into account during the design of legged systems for space exploration.

REFERENCES

1. Saranli, U., Buehler, M. and Koditschek, D.E. (2001). RHex: A Simple and Highly Mobile Hexapod Robot. *The Int. Journal of Robotics Research*, vol. 20, pp. 616-631.

2. Chacin, M. and Yoshida, K. (2008). A Microgravity Emulation Testbed for Asteroid Exploration Robots. *iSAIRAS 2008*, Hollywood, USA.

3. Bartsch, S. et al. (2010). SpaceClimber: Development of a Six-Legged Climbing Robot for Space Exploration. *ISR/ROBOTIK 2010*, Germany.

4. Kalakrishnan, K. et al (2010). Fast Robust Quadruped Locomotion over Challenging Terrain. *IEEE Int. Conference on Robotics and Automation*, Anchorage, Alaska, USA, pp. 2665-2670.

5. Gehring, C. et al (2013). Control of Dynamic Gaits for a Quadrupedal Robot. *IEEE Int. Conference on Robotics and Automation*, Karlsruhe, Germany, pp. 3287-3292.

6. Cherouveim, N. and Papadopoulos, E. (2009). Control of Hopping Speed and Height Over Unknown Terrain Using a Single Actuator. *IEEE Int. Conference on Robotics and Automation*, Kobe, Japan, pp. 2743-2748.

7. Park, H. et al (2014). Quadruped Bounding Control with Variable Duty Cycle via Vertical Impulse Scaling. *IEEE/RSJ Int. Conference on Intelligent Robots and Systems*, Chicago, Illinois, USA, pp. 3245-3252.

8. Faraji, S. et al (2013). Compliant and Adaptive Control of a planar monopod hopper in rough terrain. *IEEE Int. Conference on Robotics and Automation*, Karlsruhe, Germany, pp. 4818-4825.

9. Vasilopoulos, V., Paraskevas, I.S. and Papadopoulos, E.G. (2014). Compliant Terrain Legged Locomotion Using a Viscoplastic Approach. *IEEE/RSJ Int. Conference on Intelligent Robots and Systems*, Chicago, Illinois, USA, pp. 4849-4854.

10. Wu, A. and Geyer, H. (2014). Highly Robust Running of Articulated Bipeds in Unobserved Terrain. *IEEE/RSJ Int. Conference on Intelligent Robots and Systems*, Chicago, Illinois, USA, pp. 2558-2565.

11. Li, C., Zhang, T. and Goldman, D.I. (2013). A terradynamics of legged locomotion on granular media. *Science*, 339(6126), pp. 1408-1412.

12. Gilardi, G. and Sharf, I. (2002). Literature Survey of Contact Dynamics Modelling. *Mechanism & Machine Theory*, 37(10), pp. 1213-1239.

13. Johnson, K.L. (2000). "*Contact Mechanics*," Cambridge University Press.

14. Marhefka, D.W. and Orin, D.E. (1999). A compliant contact model with nonlinear damping for simulation of robotic systems. *IEEE Transactions on Systems, Man and Cybernetics-part A: Systems and Humans*, vol. 29, no. 6, pp. 566-572.

15. Stronge, W.J. (2000). "*Impact Mechanics*," Cambridge University Press.

16. Papadopoulos, E.G. and Chasparis, G.C. (2004). Analysis and Model-Based Control of Servomechanisms With Friction. *Journal of Dynamic Systems, Measurement and Control*, 126(4), pp. 911-915.

17. Zhu, T. [online] Some Useful Numbers on the Engineering Properties of Materials, http://goo.gl/pY8jeK.